

Microstructure Origin of Strength and Toughness of a Premium Rail Steel

A.M. Khourshid, Y.X. Gan, and H.A. Aglan

(Submitted 24 May 2000; in revised form 20 January 2001)

The mechanical properties, fracture toughness, fracture surface morphology, and failure mechanisms of different layers in a premium railhead were studied. Correlation between the mechanical properties and the failure mechanisms for each of the layers was made. It has been found that the microstructure and mechanical properties of the top layer are different from those of the inner layers, while the middle layer and the layer near the web demonstrated similar mechanical properties, microstructure, and fracture toughness. The top layer displayed 15% higher tensile strength than the other two layers. However, the strain to failure of the top layer, 11%, is only about 60% of that of the inner layers, 17.5%. The top layer has a fracture toughness, K_{Ic}, of 75 MPa m$^{1/2}$. This value for the inner layers is about 95 MPa m$^{1/2}$. Thus, the heat treatment decreases the ductility and fracture toughness of the top layer of the railhead. Transition from the brittlelike fracture mechanism of the top layer into a more ductile mechanism of the inner layers was also found.

Keywords fracture mechanisms, fracture toughness, microstructure, premium rail steel

1. Introduction

The relationship between fracture toughness and the failure behavior of rail steels is a very important aspect in the evaluation of the performance of rail steels.[1] Singh *et al.*[2] presented results on the fracture toughness behavior of standard carbon rail steel, wear resistant rail steel, and two high-strength rail steels. It has been found that higher hardness can produce lower fracture toughness. In eutectoid steels, which have the same composition as premium rail steels, it is the pearlite that controls strength, and refining the pearlite interlamellar spacing results in an increase in yield strength.[3–5] However, the effect of microstructural variables such as substructure spacing and grain size on the fracture properties of eutectoid steels is not yet clearly established. Previous studies have suggested that the fracture toughness, as determined by the Charpy impact method, is proportional to the prior austenite grain size and pearlite interlamellar spacing.[6–9] Decrease in the interlamellar spacing may increase the tendency to cleavage fracture.[10–12]

The microstructural parameters such as grain size, orientation of different phases, and texture and dimension of substructures can be changed by heat treatment. Heat treatment such as quenching is involved in the manufacturing process of premium rail steel. Due to the phase transformation related to the heat treatment, change in microstructure occurs. The railhead can be strengthened by solid solution, precipitation, and grain refining.[13] A difference in cooling speed exists at different locations inside the railhead during quenching, resulting in a considerable variation in the crystallization and grain growth kinetics of pearlite in different layers of the railhead. This in turn forms a microstructural gradient and becomes a possible origin of increased hardness and tensile strength as often found in high-strength carbon steels.[14] The microstructural effect on tensile behavior of ferrite-pearlite steels has been studied by Hussain and DelosRios.[15] The ferrite phase in the direction of maximum shear stress was identified as the preferable site for crack nucleation under tensile stress. Similar results have been reported by Nomura.[16] The sites where ferrite precipitates along austenite grain boundaries are regarded as small cracks in medium carbon ferrite pearlite steels with fine prior austenite grain size. Rosenberg and Kovove[17] investigated the effect of grain size on the brittle fracture of a medium carbon steel. The results indicated that the resistance to fracture was also dependent on the microstructure.

In the present work, the mechanical properties, fracture toughness, fracture surface morphology, and failure mechanisms of different layers in a premium rail steel were investigated. Typical specimens from representative locations were studied to identify the effect of head hardening heat treatment on the mechanical properties, fracture toughness, fracture surface morphology, and failure mechanisms. The origin of strength and toughness of the premium rail steel was identified in view of the microstructural features.

2. Materials and Experimental

The material used in the present work was a premium rail steel provided by Transportation Technology Center, Inc. (Pueblo, CO). The chemical composition range of the rail steel is given in Table 1.[18] According to the manufacturer's specification, the top of the railhead was heat-treated using air. The rail section was heated to about 780 °C and the head was air cooled immediately after hot rolling. Details of the heat treatment process can be obtained from the manufacturer.[18]

The railhead was sliced into thin layers for the preparation of test specimens. Due to head hardening of the rail, there is

A.M. Khourshid, Y.X. Gan, and **H.A. Aglan,** Department of Mechanical Engineering, Tuskegee University, Tuskegee, AL 36088. Contact e-mail: aglanh@acd.tusk.edu.

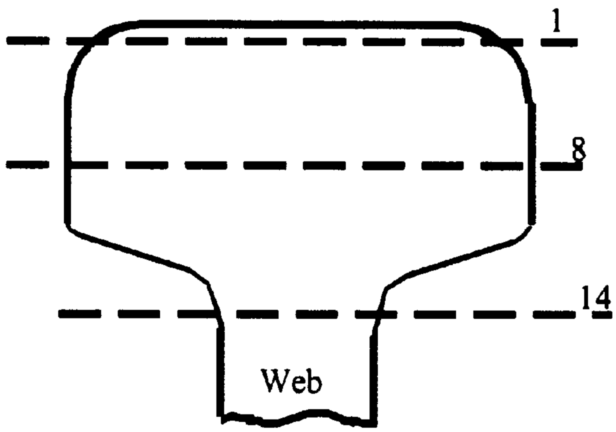

(**a**)

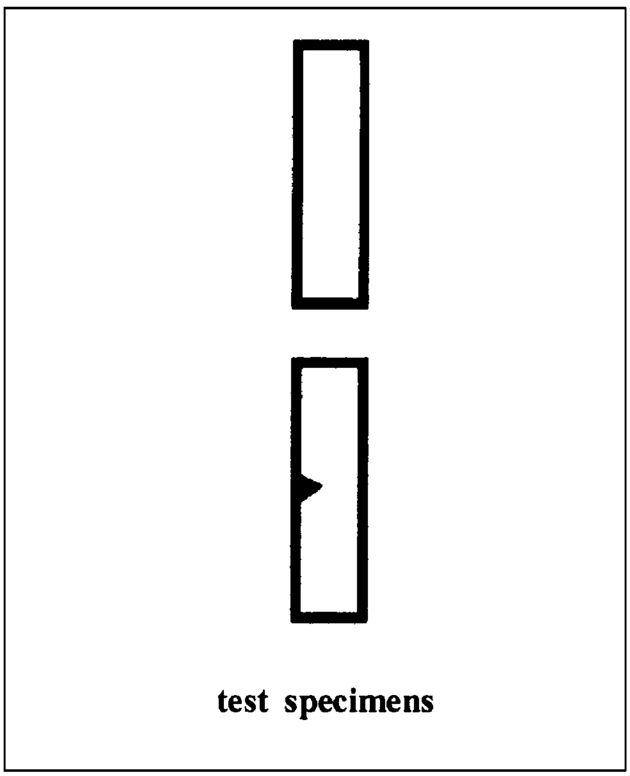

(**b**)

Fig. 1 Schematic of a railhead and a top view of slices for preparing test specimens. (**a**) Cross section of the railhead showing the location of the layers. (**b**) Top view of the slices for preparing test specimens

a vertical microstructure gradient inside the rail. Three layers were sliced from the representative locations of the railhead. One of these is the top layer (layer 1); the other two layers are below the top crust at different depths away from the top of the railhead. One was sliced from the middle of the head, layer 8, and another was at the bottom of the head, which is very close to the web, layer 14. The schematic representation of the locations of these layers is shown in Fig. 1. For the top layer of the rail, typical specimens, 50 × 5.5 × 1.2 mm, were prepared. Rectangular specimens from layers 8 and 14, 50 × 8 × 2.5 mm, were machined. Notched specimens from each layer were also prepared. At the center of one free edge of the specimens, a 60° notch was introduced using a milling machine. The notch depth to sample width ratio (a/w) was 0.43 for the specimens from the three layers.

Static tensile tests were performed using an 810 materials testing system (MTS) equipped with a 100 kN load cell. This was carried out under displacement control. The specimens were gripped between two hydraulic wedge grips of type 647.10A-01. The gage length was 25 mm. Static test results based on unnotched specimens were used to establish the stress-strain relationship, while notched specimen results were used to obtain the fracture toughness. The fracture surfaces for both notched and unnotched specimens from each layer were examined using a Hitachi (Tokyo, Japan) S-2150 scanning electron microscope operated at a maximum acceleration voltage of 25 kV. Typical micrographs revealing the fracture surface morphology were taken and recorded on Polaroid film.

3. Results and Discussion

3.1 Vertical Microstructure Gradient Inside the Railhead

The morphology of specimens from the three different layers was examined. The three layers demonstrated a microstructural gradient along the vertical direction of the railhead. Difference in the shape of grains in the top layer and the middle layer was found. The top layer consists of irregularly shaped pearlite grains due to the severe plastic deformation in the rolling procedure. Also found is the difference in the size of grains in the three layers. The middle layer and the bottom layer have an average size of 200 μm, while the top layer has smaller grains with an average about 50 μm. Since the cooling speed in the middle layer was significantly smaller than that of the top layer during the head hardening process, a greater supercooling state can be established in the top layer. The tendency of crystal initiation in the top layer is much higher than that in the middle layer. However, the equilibrium growth process cannot be finished due to the fast cooling. Thus, the grain size in the top layer is smaller than that in the middle layer or the bottom layer. Larger spacing between the substructures of ferrite and cementite laminae in the middle layer than that of the top layer was found as well. Such a difference can also be explained by the difference in the kinetics of pearlite growth. Faster cooling normally results in finer pearlite grains and smaller space between the substructure of ferrite and cementite in the pearlite crystals.

3.2 Microstructure Dependence of Strength and Fracture Toughness

The mechanical properties for each layer are given in Table 2. Each of the values quoted is the mean of at least three tests. Both tensile and fracture toughness tests were carried out at room temperature.

Stress-strain relationships for unnotched specimens from the three different layers, 1, 8, and 14, are shown in Fig. 2. It should be mentioned that all specimens were tested along the rolling direction of the rail, *i.e.*, in the traffic direction. It can be seen from Fig. 2 that there is a difference in the properties

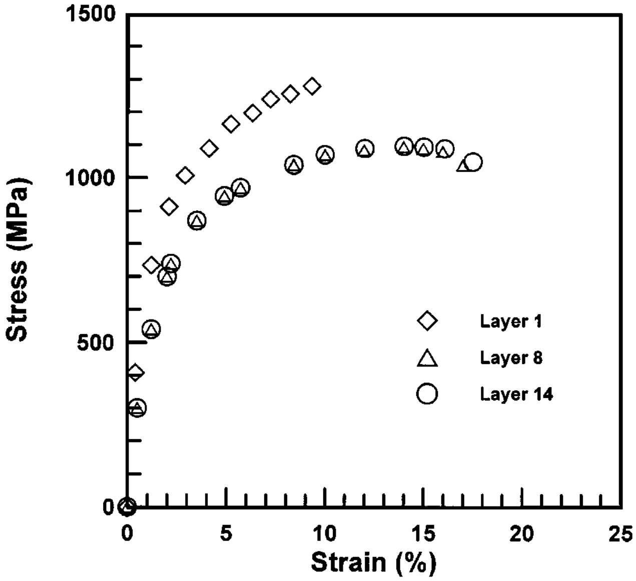

Fig. 2 Stress-strain relationship of unnotched specimens for the three layers from the railhead

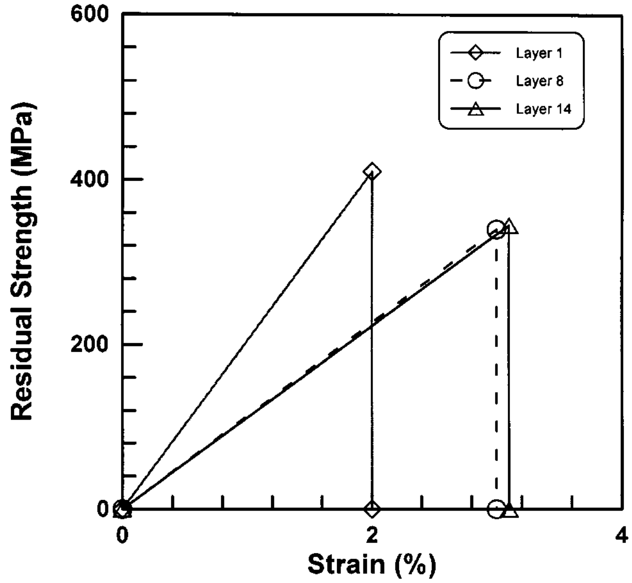

Fig. 3 Stress-strain relationship of notched specimens for the three layers from the railhead

Table 1 Chemical composition of the premium rail steel[18]

Element	C	Mn	P	S	Si	Ni	Cr	Mo	V
Content, wt.%	0.72–0.78	0.60–1.25	0.035	0.037	0.10–0.60	0.25	0.25–0.50	0.10	0.03–0.05

Table 2 Mechanical properties and fracture toughness for different layers from the rail head

Ultimate strength, σ_u (MPa)	1280	1092	1097
Strain to failure, ε (%)	11	17.5	18
Fracture toughness K_{Ic} (MPa $\sqrt{m}$)	75	95	92

between layer 1 and both layers 8 and 14. Both layers 8 and 14 have, almost, the same ultimate strength and strain to failure. Thus, it appears that the heat treatment of the railhead has affected only the top layer, which is about 5 mm from the top surface of the head. The increase in the ultimate strength and decrease in the strain to failure will cause the top of the rail to resist deformation due to the repetitive load applications from the wheels of passing trains. The fracture toughness K_{Ic} was calculated from Fig. 3 and the following linear elastic fracture mechanics equation: $K_{Ic} = \sigma_c \sqrt{a}\, F(a/W)$, where σ_c is the residual stress, a is the initial crack length, and $F(a/w)$ is a geometrical correlation factor.[19] As can be seen from Fig. 3, the notched behaviors of the rail steel at the three different locations from the railhead display linear elastic fracture. The value of K_{Ic} for the top layer was found to be 75 MPa $\sqrt{m}$, and for layers 8 and 14, the values of K_{Ic} were 95 and 92 MPa $\sqrt{m}$, respectively. It is evident that the difference between the fracture toughnesses of layers 8 and 14 is negligible. However, there is a noticeable difference between layer 1 and both layers 8 and 14. The ratio of the fracture toughness between layer 1 and both layers 8 and 14 is about 0.8.

The relationship between tensile stress and toughness can be complex. For example, in various heat treatment conditions, the plain strain fracture toughness increases as the tensile ductility decreases.[5] Thus, it is important to consider the end-use application of the material when a heat treatment is considered. For example, the tensile ductility may be relevant to the bend formability of a crack-free piece of steel, but would be of no significance for assessing the susceptibility of the steel to the presence of cracklike defects.

The variation of strength from layer 1 to layer 8 with microstructure indicates a distinct effect of interlamellar spacing and prior austenite grain size. The exact mechanisms controlling this effect are not known. Austenitic grain size,[19] pearlite colony size,[3] and pearlite spacing[20] have all previously been correlated with toughness. Miller and Smith[21] studied tensile specimens and observed that, as the austenite to pearlite transformation temperature was changed from 692 to 705 °C, the number of pearlite shear cracks decreased. This was attributed to the fact that the transformation produced a finer, harder pearlite with smaller interlamellar spacing. The work of Hyzark and Bernstein[22] also supports this relation between lamellar spacing and strength. There has been only limited attention paid to the relationships between strength and mechanical properties of lamellar microstructure materials. Most of this research has focused on *in-situ* composites.[23] More details have been reported concerning the mechanical behavior of pearlite structure.[24,25] For example, Lawson and Kerr[24] have found that the rate of matrix hardening during monotonic loading increased

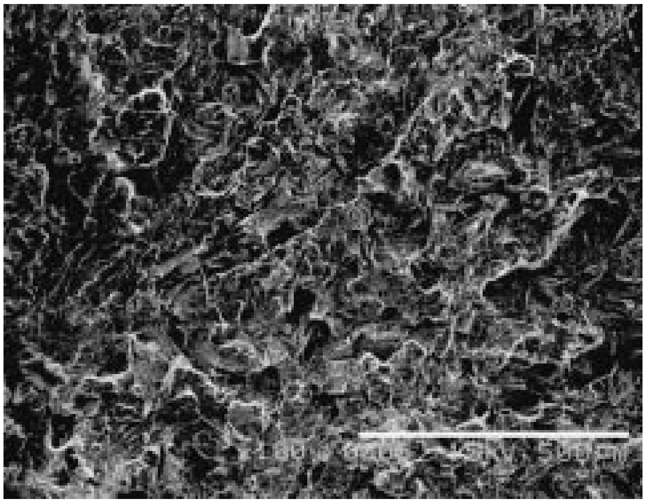

Fig. 4 Fractograph at 100× showing the failure mechanism of an unnotched specimen from the top layer of the railhead

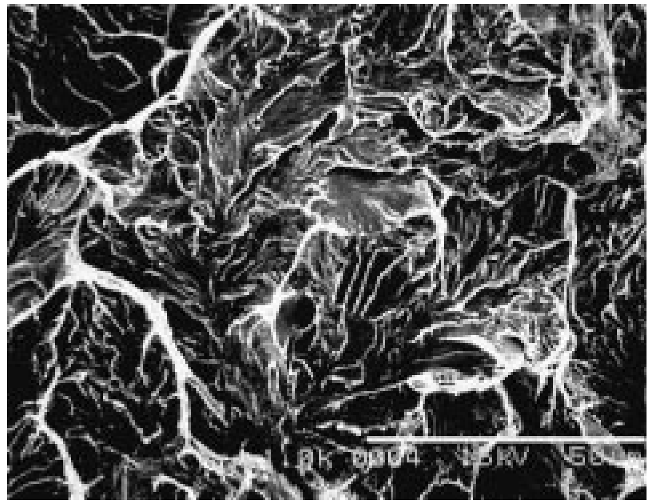

Fig. 5 Fractograph at 1000× showing the failure mechanism of an unnotched specimen from the top layer of the railhead

with decreasing laminae spacing, in other metallic materials. Similar results have been reported by Aita and Weertman,[26] namely, that the ductile failure of the matrix was followed by fracture of the brittle laminae.

3.3 Microstructure Dependence of Fracture Mechanisms

The fracture surface morphology of different layers from the railhead were examined to identify the microstructure origin of strength and toughness. The middle layer and the layer near the web demonstrated similar mechanical properties and fracture toughness, as shown in Table 2. It is also noticed that the microstructural features for both layers 8 and 14 are similar. Thus, microscopic analysis was focused on the comparative studies of the top layer (layer 1) and the middle layer (layer 8). The fracture surface of unnotched specimens was examined using scanning electron microscopy (SEM) at 100 and 1000×, while the notched specimens were examined at 1000×.

The micrograph of Fig. 4 shows the morphology of the fracture surface of an unnotched specimen from layer 1 at 100×. It can be seen that a number of transgranular microcracks exist on the fracture surface. At higher magnification, Fig. 5 at 1000×, it can be seen these cracks are cutting right across the pearlite colonies, along the orientation of the cleavage planes of the ferrite. Some of these colonies fracture along the interface between cementite and ferrite. The fracture surfaces show large flat facets mixed with regions with large differences in elevation. The laminae pearlite structure may be distinguished in most areas as a striated pattern, as shown in Fig. 5 for the top layer. The laminae are often crossed by tear ridges forming a type of river marking, though these are not so distinct as on regular one-phase cleavage facets.

Layer 8 displayed a considerable amount of plastic deformation before failure, as shown in Fig. 6, which is an SEM micrograph at 100×. The density of microcracks on the fracture surface is quite low compared with Fig. 4 for the top layer. Pulled up material, large voids, and tearing features can be seen. Figure 7 at 1000× shows a location that is thought to be an initiation site of a cleavage facet. Further details can be seen

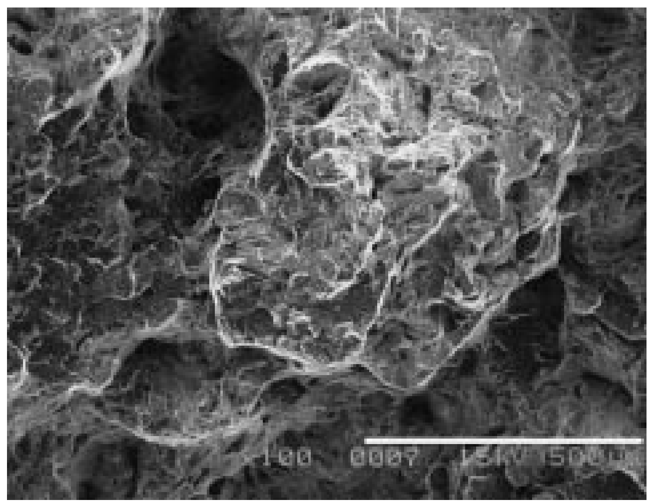

Fig. 6 Fractograph at 100× showing the failure mechanism of an unnotched specimen from the middle layer of the railhead

from the left side of the micrograph in Fig. 7. River patterns radiate outward from this location and indicate the local direction of propagation of the cleavage crack from left to right. It is evident that the propagation direction may be at an angle to the lamellae as well as parallel to them, but the ridges have a tendency to bend locally, following the lamellae for a short distance, indicating that crack propagation is somewhat easier parallel than perpendicular to the lamellae. Occasionally, the crack follows the cementite-ferrite phase boundary for short distances. The micrographs at 1000× in Fig. 5 and 7 for layers 1 and 8, respectively, indicate that the pearlite colony boundaries or prior austenite grain boundaries may act as obstacles to a growing cleavage crack.

Notched specimens fractured under tensile loading were also examined. The fracture surface can be divided into two regions based on the morphological features: a crack initiation region followed by a fast crack growth region. In the first region,

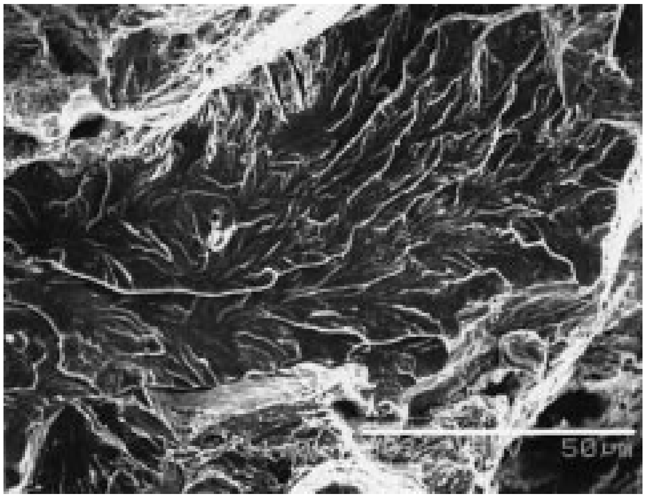

Fig. 7 Fractograph at 1000× showing the failure mechanism of an unnotched specimen from the middle layer of the railhead

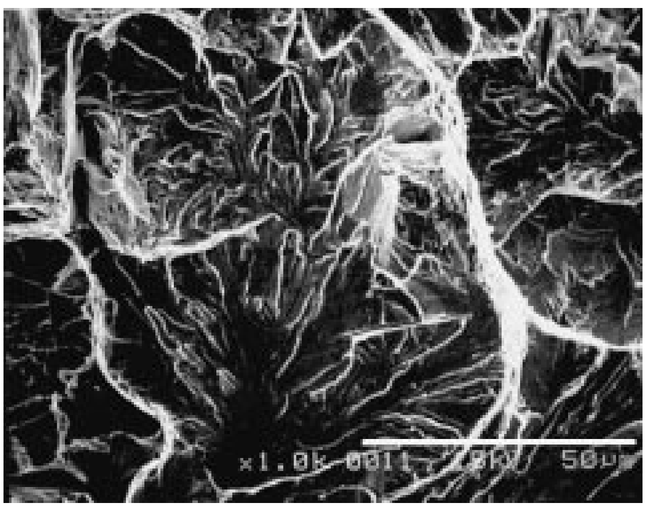

Fig. 8 Fractograph at 1000× showing the crack initiation region of the top layer of the railhead. The prenotch is located at the left side of the micrograph

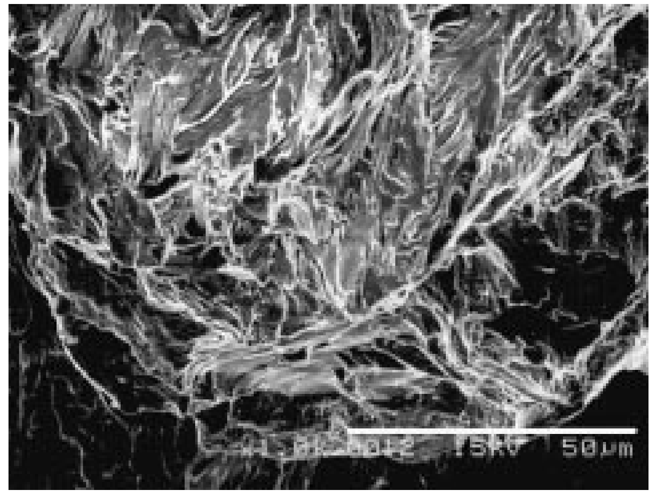

Fig. 9 Fractograph at 1000× showing the crack initiation region of the middle layer. The prenotch is located at the left side of the micrograph

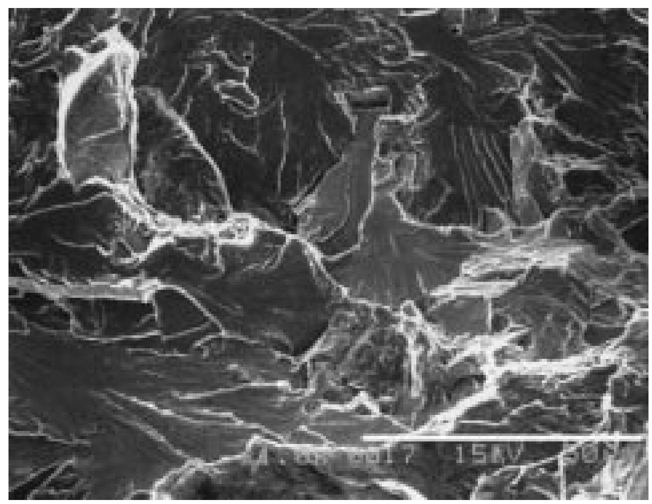

Fig. 10 Fractograph at 1000× showing the region of fast crack propagation of the top layer. The crack growth direction is from left to right

the top layer exhibited "river lines," which enabled fracture initiation sites to be located, as shown in Fig. 8. The fracture in this area was probably triggered by a defect such as an inclusion. The cleavage fracture near the notch root, the far left of the micrograph, revealed sub-notch-root fracture initiation sites. Cleavage river lines emanated both toward the notch as well as away from it, as shown in the lower part of Fig. 8. All of these features indicate a brittle mechanism in the crack initiation region. The fracture surface of a typical notched tensile specimen from the middle layer (layer 8) exhibits a ductile fracture mechanism. The fracture surface in the first region of crack initiation displayed void coalescence, as shown in Fig. 9. The ductile mechanism was further detailed by the pulled-up material and tearing ridgelines inside a grain. Well-drawn ferrite strips can be seen on the entire fracture surface. Such features are obviously different from those on the fracture surface of the top layer in which cleavage features are predominant.

The fracture surface features in the second region for both layers 1 and 8 are shown in Fig. 10 and 11, respectively. Fast crack growth features are easily seen in such locations far away from the notch tip. For the specimen from the top layer, Fig. 10 at 1000×, this region shows a mixed type of fracture mechanism with the brittle mechanism as the dominant one. In Fig. 10, the well-pronounced cleavage facets and river markings are shown in addition to the less dominant ductile tearing features such as pulled-up ferrite strips and tearing ridges. In some particular areas such as in the upper right corner and lower left part of Fig. 10, the cleavage orientation and secondary crack propagation direction could readily be followed from facet to facet. This allows the fracture path to be traced to find the

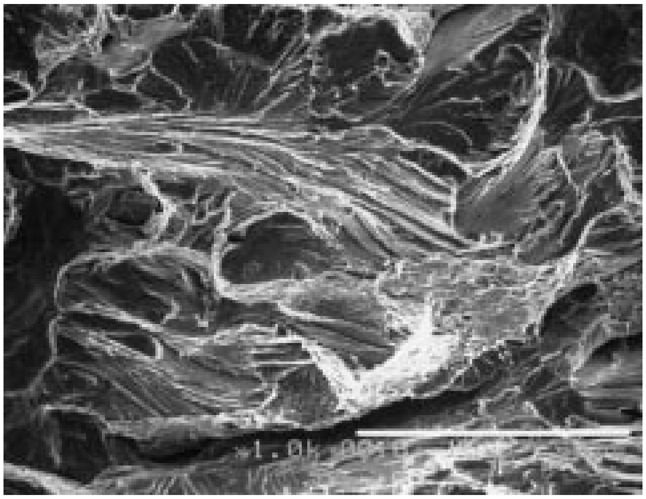

Fig. 11 Fractograph at 1000× showing the region of fast crack propagation of the middle layer from the railhead. The crack growth direction is from left to right

cleavage origin, as marked by the radial pattern of river lines in these areas in Fig. 10. In contrast with the top layer, the middle layer demonstrated significant plasticity in this region, as shown in Fig. 11, which shows a micrograph at 1000× for the fracture surface. A dimpled fracture surface was presented along grain boundaries, as can be seen from the lower right part of the fracture surface. Pulled-up material in this micrograph reveals a large amount of plastic deformation associated with the crack growth. Tearing inside the grains was also shown. The laminate separation between ferrite and cementite can be seen in some particular sites, as shown in the upper left part of Fig. 11. Obviously, a ductile fracture mechanism is dominant in the notched specimen from the middle layer of the premium railhead.

4. Conclusions

- The microstructure and mechanical properties of the top layer are different from those of the inner layers, while the middle layer and the layer near the web demonstrated similar mechanical properties, microstructure, and fracture toughness.
- The head hardening heat treatment decreases the ductility of the top layer of the railhead. The top layer has a tensile strength of 1280 MPa, which is about 15% higher than the other two layers. However, the strain to failure of the top layer, 11%, is only about 60% of that of the inner layers, 17.5%.
- A decrease in fracture toughness due to the head hardening was found. The top layer has a fracture toughness, K_{Ic}, of 75 MPa $m^{1/2}$. This value for the inner layers is about 95 MPa $m^{1/2}$.
- Transition from a brittlelike fracture mechanism for the top layer to a more ductile mechanism for the inner layers is revealed by the microscopic examination on the fracture surface morphology of these layers.

Acknowledgments

This work was supported by the Federal Railway Administration, United States Department of Transportation (DOT). The guidance and support of the FRA technical monitor, Mr. M. Fateh, is greatly appreciated. Tyrone Harper, a senior undergraduate student at Tuskegee University, is also acknowledged for the preparation of the specimens.

References

1. I. Vitez: *Metalurgija,* 1996, vol. 35, p. 49.
2. U.P. Singh, R. Singh, and S. Banerjee: *Scandina J. Metall.,* 1995, vol. 24, p. 237.
3. T. Gladman, I. McIvor, and F. Pickering: *J. Iron Steel Inst.,* 1972, vol. 210, p. 916.
4. M. Gensamer, E.B. Pearsall, W.S. Pellini, and J.R. Low, Jr.: *Trans. ASM,* 1942, vol. 30, p. 983.
5. T. Takahashi and M. Nagumo: *Trans. Jpn. Inst. Met.,* 1970, vol. 11, p. 113.
6. J.M. Hyzak and I.M. Bernstein: *Metall. Trans. A,* 1976, vol. 7A, p. 1217.
7. G. Langford: *Metall. Trans. A,* 1977, vol. 8A, p. 861.
8. D. Porter, K. Easterling, and G. Smith: *Acta Metall.,* 1978, vol. 26, p. 1405.
9. G.K. Bouse, I.M. Bernstein, and D.H.Stone: in *Rail Steel Development, Processing and Use,* ASTM Standard STP 644, D.H. Stone and G.G. Knupp, eds., ASTM, Philadelphia, PA, 1978, pp. 145-66.
10. F.P.L. Kavishe and T.J. Baker: *Mater. Sci. Technol.,* 1986, vol. 2, p. 816.
11. F.P.L. Kavishe and T.J. Baker: *Mater. Sci. Technol.,* 1986, vol. 2, p. 583.
12. J.J. Lewandowski and A.W. Thompson: *Proc. 6th. Int. Conf. on "Fracture,"* S.R. Valluri *et al.*, eds., Pergamon Press, Oxford, United Kingdom, 1984, p. 1515.
13. M. Kurita, K. Toyama, and T.T. Hagane: *J. Iron Steel Inst. Jpn.,* 1994, vol. 80, p. 66.
14. J.C. Shin, S. Lee, and J.H. Ryu: *Int. J. Fatigue,* 1999, vol. 21, p. 571.
15. K. Hussain and R.R. DelosRios: *J. Mater. Sci.,* 1997, vol. 32, p. 3565.
16. I. Nomura: *J. Iron Steel Inst. Jpn.,* 1997, vol. 83, p. 227.
17. G. Rosenberg and M. Kovove: *Metallic Mater.,* 1996, vol. 34, p. 201.
18. *AREA Manual for Railway Engineering,* American Railway Engineering Association, Pueblo, CO, 1997, p. 4.
19. A. Turkalo: *Trans. TMS-AIME,* 1960, vol. 218, p. 24.
20. G. Burns and C. Judge: *J. Iron Steel Inst.,* 1956, vol. 194, p. 333.
21. L.E. Miller and G.C. Smith: *J. Iron Steel Inst.,* 1970, vol. 208, p. 998.
22. K.J. Sawley and D.D. Davis: *Technology Digest,* Association of American Railroads, Pueblo, CO, Nov. 1996.
23. C.H. Henager, Jr. and J.L. Brimhall: in *In-situ Composites: Science and Technology,* M. Singh and D. Lewis, ed., The Minerals, Metals and Materials Society, Warrendale, PA, 1993, pp. 61-80.
24. W.H. Lawson and H.W. Kerr: *Metall. Trans.,* 1971, vol. 2, p. 2853.
25. W.R. Hoover and R.W. Hertzburg: *Trans. ASM,* 1968, vol. 61, p. 769.
26. C.R. Aita and J. Weertman: *Metall. Trans. A,* 1979, vol. 10A, p. 535.